

Molecular Dynamics Simulations of Forced Unbending of Integrin $\alpha_V\beta_3$

Wei Chen^{1‡a}, Jizhong Lou^{2‡b}, Jen Hsin³, Klaus Schulten³, Stephen C. Harvey^{2,4}, Cheng Zhu^{1,2,5*}

1 Woodruff School of Mechanical Engineering, Georgia Institute of Technology, Atlanta, Georgia, United States of America, **2** Institute for Bioengineering and Bioscience, Georgia Institute of Technology, Atlanta, Georgia, United States of America, **3** Department of Physics and Beckman Institute, University of Illinois at Urbana-Champaign, Urbana, Illinois, United States of America, **4** School of Biology, Georgia Institute of Technology, Atlanta, Georgia, United States of America, **5** Coulter Department of Biomedical Engineering, Georgia Institute of Technology, Atlanta, Georgia, United States of America

Abstract

Integrins may undergo large conformational changes during activation, but the dynamic processes and pathways remain poorly understood. We used molecular dynamics to simulate forced unbending of a complete integrin $\alpha_V\beta_3$ ectodomain in both unliganded and liganded forms. Pulling the head of the integrin readily induced changes in the integrin from a bent to an extended conformation. Pulling at a cyclic RGD ligand bound to the integrin head also extended the integrin, suggesting that force can activate integrins. Interactions at the interfaces between the hybrid and β tail domains and between the hybrid and epidermal growth factor 4 domains formed the major energy barrier along the unbending pathway, which could be overcome spontaneously in $\sim 1 \mu\text{s}$ to yield a partially-extended conformation that tended to rebend. By comparison, a fully-extended conformation was stable. A newly-formed coordination between the α_V Asp457 and the α -genou metal ion might contribute to the stability of the fully-extended conformation. These results reveal the dynamic processes and pathways of integrin conformational changes with atomic details and provide new insights into the structural mechanisms of integrin activation.

Citation: Chen W, Lou J, Hsin J, Schulten K, Harvey SC, et al. (2011) Molecular Dynamics Simulations of Forced Unbending of Integrin $\alpha_V\beta_3$. PLoS Comput Biol 7(2): e1001086. doi:10.1371/journal.pcbi.1001086

Editor: Emanuele Paci, University of Leeds, United Kingdom

Received: August 17, 2010; **Accepted:** January 18, 2011; **Published:** February 17, 2011

Copyright: © 2011 Chen et al. This is an open-access article distributed under the terms of the Creative Commons Attribution License, which permits unrestricted use, distribution, and reproduction in any medium, provided the original author and source are credited.

Funding: This research was supported by NIH grants AI44902 (C.Z.) and P41-RR05969 (K.S.). The funders had no role in study design, data collection and analysis, decision to publish, or preparation of the manuscript.

Competing Interests: The authors have declared that no competing interests exist.

* E-mail: cheng.zhu@bme.gatech.edu

‡a Current address: Department of Bioengineering, University of Washington, Seattle, Washington, United States of America

‡b Current address: National Laboratory of Biomacromolecules, Institute of Biophysics, Chinese Academy of Sciences, Beijing, China

Introduction

Integrins are $\alpha\beta$ heterodimeric transmembrane receptors for cell-cell and cell-extracellular matrix adhesions [1]. The overall shape of an integrin ectodomain is that of a large head supported by two long legs [2,3]. The head of αA (or αI) domain-lacking integrins, including the integrin $\alpha_V\beta_3$ studied here, consists of the β -propeller domain of the α subunit and the βA (or βI) domain of the β subunit (Fig. 1A). The two legs contain the thigh domain and the calf-1 and -2 domains of the α subunit and the hybrid, plexin-semaphorin-integrin (PSI), epidermal growth factor (EGF) 1–4 domains and the β tail domain (βTD) of the β subunit.

Under physiological conditions, integrins may assume an inactive state with low affinities for ligands. Upon activation by extracellular or intracellular stimuli, they may change conformations and bind ligands with high affinities and transduce signals across the plasma membrane [1]. A bent conformation, where the legs are bent at the knees, or genua, between the thigh and calf-1 domains of the α subunit and between the EGF1 and EGF2 domains of the β subunit to allow the N-terminal headpiece (from the N-termini to the knees) to contact the C-terminal tailpiece (from the knees to the C-termini) (Fig. 1A), was observed in all published crystal structures of complete integrin ectodomains, including $\alpha_V\beta_3$ [4–7], $\alpha_{IIb}\beta_3$ [8], and $\alpha_X\beta_2$ [9]. In contrast to the “closed” headpieces observed in these bent integrins, crystal

structures of an integrin $\alpha_{IIb}\beta_3$ headpiece adopt an open conformation with the hybrid domain swinging out $\sim 60^\circ$ [10]. Electron microscopy (EM) studies have observed different global conformations for integrins under different conditions, including a bent conformation, an extended conformation with a closed headpiece, and an extended conformation with an open headpiece [11–13]. A switchblade model has been proposed such that integrins undergo large global conformational changes from bent to extended during activation [11,14]. Alternatively, a deadbolt model suggests much smaller conformational changes such that the CD loop (the β hairpin loop between the β strands C and D) of the βTD acts as a regulable deadbolt, the relief of which unlocks the βA domain from the inactive state [15].

As transmembrane mechanical links between intracellular and extracellular environments [1], integrins are often subjected to tensile forces applied externally at the head, where ligands bind, or internally at the cytoplasmic tail, where the cytoskeleton attaches. It seems intuitive that such pulling force may straighten a bent integrin and even induce other forms of conformational changes, leading to integrin activation. Indeed, force has been shown to strengthen integrin-mediated adhesion [16,17] and prolong integrin-ligand bond lifetimes [18,19].

Computational approaches, especially molecular dynamics (MD), have been used to study force-induced integrin conformational changes. These included steered MD (SMD) to simulate the

Author Summary

Proteins can regulate their functions via conformational changes. One example is integrins, which are transmembrane receptors mediating cell-cell and cell-matrix adhesions. Inactive integrins may assume a bent conformation with low affinities for ligands unable to support adhesions. Intracellular or extracellular stimuli induce large scale changes from the bent to an extended conformation, resulting in active integrins with high affinities for ligands to mediate strong adhesions. We used molecular dynamics simulations to reveal the dynamics and pathways of integrin unbending in atomic details. Critical interactions in this process were identified. This study not only sheds light on the structural mechanisms of integrin activation, but also exemplifies allosteric regulations of protein functions.

swing-out in the headpieces of both integrin $\alpha_V\beta_3$ and $\alpha_{IIb}\beta_3$ [23], NMA to investigate the unbending of the ectodomain of integrin $\alpha_V\beta_3$ that lacks the PSI, EGF1, and EGF2 domains at the knee region [24], and SMD to simulate the conformational change between the closed and open legs on an extended model of the complete ectodomain of integrin $\alpha_{IIb}\beta_3$ [8].

Extending from these studies, we performed all-atom, explicit-solvent MD simulations for the complete ectodomain of integrin $\alpha_V\beta_3$ in both unliganded and liganded forms. Constant-velocity pulling of the head gradually unbent the integrin without major distortions of individual domains. Constant-force pulling induced a rapid transition from the bent to extended conformation after a waiting time, which increased exponentially with decreasing force to extrapolate to $\sim 1 \mu s$ at zero force. Two groups of interactions between the headpiece and tailpiece of the β_3 subunit have been identified as the major barrier along the unbending pathway. A partially-extended conformation was observed to spontaneously bend back. A fully-extended conformation remained straight, which might be stabilized at least partly by a new coordination between Asp457 of the α_V subunit and the metal ion at the α -genou. Pulling the bound ligand also unbent the integrin, suggesting that force can activate integrins.

opening of the $\alpha_V\beta_3$ headpiece [20,21], targeted MD (TMD) and normal mode analysis (NMA) to study the conformational change of the β_3 headpiece [22], TMD to simulate the hybrid domain

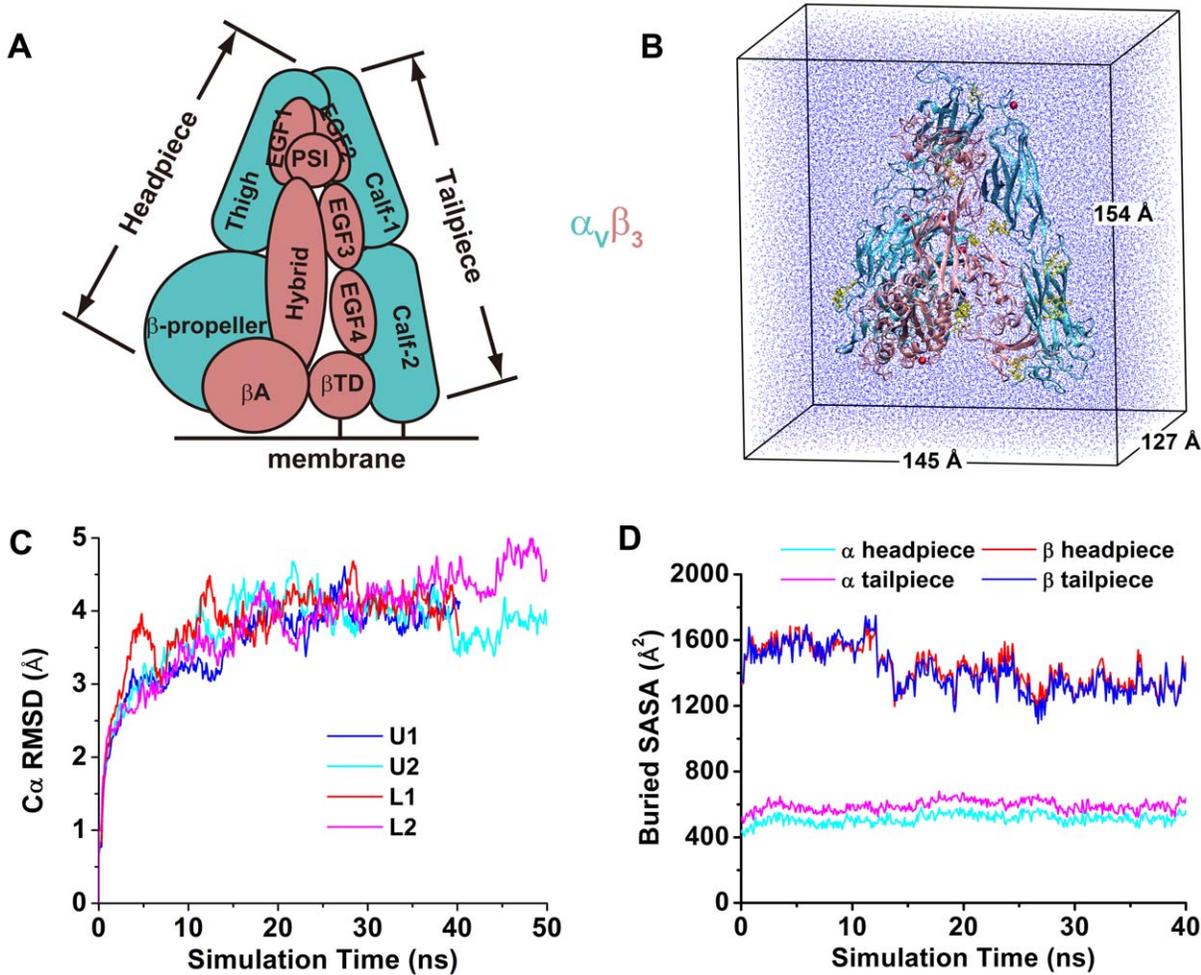


Figure 1. System equilibration. **A.** Schematic of an extracellular portion of integrin $\alpha_V\beta_3$ showing the various domains of the α_V (cyan) and β_3 (pink) subunits. **B.** Structure of U1 in a water box used for equilibration with the integrin subunits shown in the same color scheme as in panel A. Yellow sticks represent sugars attached on the protein. Red spheres represent divalent metal ions bound to the protein. Blue dots represent water molecules. The same color codes and representations are used in all figures and videos. **C.** C_α RMSDs of the four simulated structures during equilibration. **D.** Buried SASAs between the headpiece and tailpiece of U1 during equilibration. doi:10.1371/journal.pcbi.1001086.g001

Results

Equilibration of integrin $\alpha_V\beta_3$ systems

The present work includes a total of >600 ns all-atom, explicit-solvent MD simulations for four complete integrin $\alpha_V\beta_3$ ectodomains (Table S1): two unliganded (U1 and U2) and two liganded forms with a cyclic RGD peptide (L1 and L2). During equilibration in a small water box (Fig. 1B), the root-mean-square deviations (RMSDs) of all C α atoms (C α RMSDs) first increased and then leveled off at ~ 4 Å (Fig. 1C), indicating that equilibrium had been reached. All four equilibrated structures assumed a bent conformation with many contacts between the headpiece (α_V residues 1–600 and β_3 residues 1–472) and tailpiece (α_V residues 601–956 and β_3 residues 473–690). The calculated buried solvent-accessible surface areas (SASAs) between the headpiece and tailpiece indicate much more extensive contacts of the β_3 subunit than the α_V subunit (Fig. 1D). The major barrier to unbending is therefore expected to come from the β_3 subunit.

Unbending of unliganded integrin $\alpha_V\beta_3$ by constant-velocity SMD

We used constant-velocity SMD simulations [25] to accelerate integrin unbending. The enlarged systems with bigger water boxes to accommodate unbending (Fig. 2A) were first equilibrated using 4–8 ns free dynamics. A force was then applied to the head of the unliganded integrin $\alpha_V\beta_3$ (U1 or U2), where ligand-binding sites are, by a spring moving at a constant velocity while the β TD was constrained to mimic the membrane anchorage (Fig. 2B). The α -leg was not constrained to allow separation of two legs, should it occur. Regardless of the initial pulling directions, force became aligned along the direction from the constraint location to the pulling location after the integrin underwent a rigid-body rotation. Remarkably, pulling readily caused gradual unbending of integrin $\alpha_V\beta_3$ without major distortions of its individual domains, resulting in a fully-extended conformation with a closed headpiece and closed legs (Fig. 2C and Videos S1 & S2).

Setting the pulling speed $v = 2$ nm ns⁻¹ and the spring constant $k = 0.5$ kcal mol⁻¹ Å⁻², we varied the pulling direction by loading force at different locations: β A, β -propeller, or both. Interestingly, regardless of where force was loaded, a major force peak occurred at ~ 2 nm extensions (defined as the increase of distance between the constraint and pulling locations) (Fig. 2D). Setting the pulling direction by pulling the β A domain, we next varied the pulling speed from 0.5 to 10 nm ns⁻¹ and the spring constant from 0.1 to 1 kcal mol⁻¹ Å⁻² (Fig. 2E). At $v = 10$ nm ns⁻¹ and $k = 1$ kcal mol⁻¹ Å⁻², the pulling force rapidly increased to $\sim 1,000$ pN at the peak level, indicating a large viscous resistant to high speed extension. At $v = 0.5$ nm ns⁻¹, the force fluctuations with $k = 0.1$ kcal mol⁻¹ Å⁻² were much smaller than those with $k = 0.5$ kcal mol⁻¹ Å⁻², as expected. Importantly, a major force peak was observed at similar extensions regardless of the pulling parameters. After the major peak, force dropped to a much lower level until the integrin was straightened. These results suggest that the unbending pathway was unchanged for the different pulling parameters tested. In the following simulations, we applied force to the β A domain and chose a medium pulling speed of 2 nm ns⁻¹ and a medium spring constant of 0.5 kcal mol⁻¹ Å⁻² unless otherwise indicated.

To assess the robustness of the results, we repeated constant-velocity SMD simulations three times (U1 SMD 1–3) with different equilibrated U1 structures and observed well-aligned force-extension curves with force peaks of comparable heights and at similar extensions (Fig. 2F). We also performed one constant-velocity SMD simulation for an equilibrated U2 structure (U2

SMD) and observed two major force peaks at the same extension range where the single force peaks were seen in the U1 simulations (Fig. 2F).

To elucidate the cause of the major force peak(s), we analyzed the buried SASAs and hydrogen bonds (H-bonds) between the headpiece and tailpiece for different integrin domains (Fig. 3). The decrease in the buried SASAs of different domains during integrin unbending revealed the disruption of interdomain interactions as the originally buried surfaces were exposed. The drops of the buried SASAs of the hybrid, β TD, and EGF4 domains were found to coincide with the major force peak (Figs. 3 and S1), identifying the interactions at the hybrid/ β TD and hybrid/EGF4 interfaces as the major barrier to unbending. Interactions between the β A domain and β TD also contributed to the major force peak for U2, but these interactions were broken spontaneously during the equilibration of U1 and thus not seen in the U1 SMD simulations (cyan curves in Figs. 3 and S1). In the U1 SMD 1 & 2, interactions at the two interfaces were broken at the same time. However, in the U1 SMD 3 and the U2 SMD, interactions at the hybrid/ β TD interface were broken before those at the hybrid/EGF4 interface, giving rise to a small bump after the major force peak in the U1 SMD 3 and splitting the major force peak into two in the U2 SMD (gray curves in Figs. 3 and S1).

The hybrid/ β TD interface was bound mainly by polar interactions, including a salt bridge between Asp393 and Arg633 (Figs. 4 A & B) as well as H-bonds whose number decreased from 8 to 0 as the simulations passed the major force peak (Figs. 3 and S1). In contrast, the hybrid/EGF4 interface was bound mainly by hydrophobic interactions, involving several nonpolar residues (Leu375, Ile380, Leu383, Met387, Met568, Leu573, and Leu574) (Figs. 4 C & D). In addition to the hydrophobic interactions, several H-bonds were observed at the hybrid/EGF4 interface for U2 (Fig. S2).

To examine whether the forced extension of the two knees occurred cooperatively, we analyzed three hinge angles: the thigh/calf-1 hinge angle for the α -knee and the EGF1/EGF2 and EGF2/EGF3 hinge angles for the β -knee (Figs. 5 and S3). Both the EGF1/EGF2 and EGF2/EGF3 hinges are bent in the starting structure of U1 (where the EGF1 and EGF2 domains were modeled) (Fig. S4); hence, these hinge angles opened significantly during integrin extension. In the starting structure of U2, by comparison, the β -knee is mainly bent at the EGF1/EGF2 hinge and hence this was where the major angle changes occurred. The hinge angles for the α - and β -knees increased with increasing head-tail extension concurrently (Figs. 5 and S3 A & B). To examine their cooperation, different hinge angles were plotted against each other, which reveal linear relationships until the integrin was over-stretched beyond the point where the integrin was fully straightened and the flexible EGF domains began to rotate about different hinges (Figs. 5 and S3 C & D). These results indicate that the interactions that hold the α/β knees in the bent conformation are cooperative.

Unbending of unliganded integrin $\alpha_V\beta_3$ by constant-force SMD

To complement and compare with the constant-velocity SMD simulations, we performed a series of constant-force SMD simulations for U1 and U2, where constant forces were loaded to the β A domain along the same direction with the β TD constrained as before. Instead of repeating the simulations at the same force, we used five forces from 97–195 pN for U1 and a 195 pN force for U2. Upon application of force, the head-tail distance was held at 4–5 nm initially, indicating the stability of the bent conformation, then increased suddenly, indicating a rapid

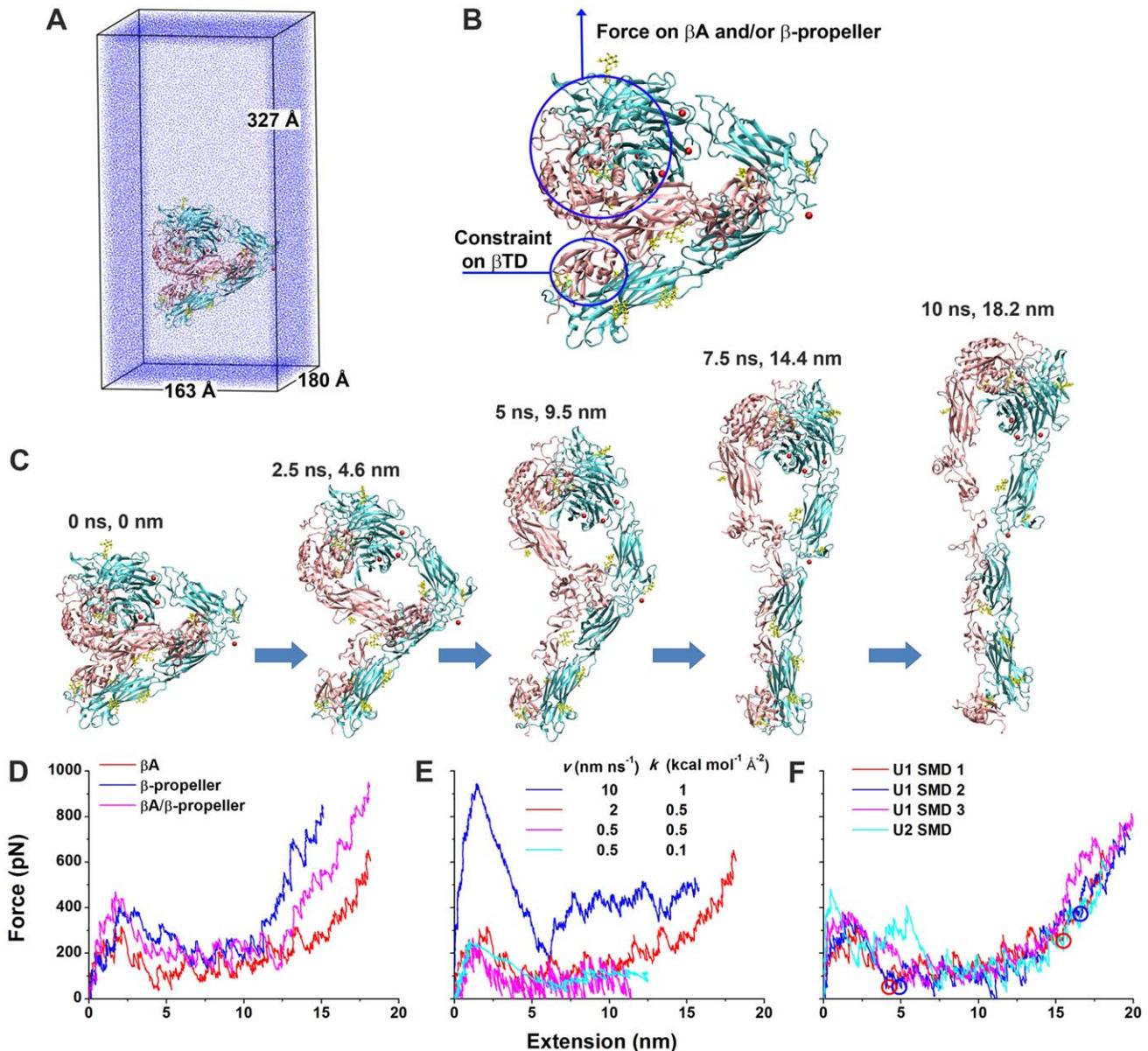


Figure 2. Forced unbending of unliganded integrin $\alpha_v\beta_3$. **A.** U1 in the enlarged water box for unbending simulations. **B.** Illustration of force application on the head and constraint on the βTD in the SMD simulations of U1 and U2. **C.** Snapshots of a representative unbending process (U1 SMD 1) taken at indicated times and extensions. **D.** Force-extension curves in the constant-velocity SMD simulations of U1 by pulling the βA and/or β -propeller domains with a 2 nm ns⁻¹ pulling speed and a 0.5 kcal mol⁻¹ Å⁻² spring constant. **E.** Force-extension curves in the constant-velocity SMD simulations of U1 by pulling the βA domain with indicated pulling speeds and spring constants. **F.** Force-extension curves for three constant-velocity SMD simulations of U1 and one constant-velocity SMD simulation of U2 with a 2 nm ns⁻¹ pulling speed and a 0.5 kcal mol⁻¹ Å⁻² spring constant. Red and blue circles indicate respective structures along the unbending pathways from the trajectories of the U1 SMD 1 & 2 that were selected as starting structures for free MD simulations. The left two represent partially-extended structures and the right two represent fully-extended structures. The red curves in panels D–F are all for the U1 SMD 1. doi:10.1371/journal.pcbi.1001086.g002

conformational transition, and finally leveled off, indicating full extension (Fig. 6A). The rapid transition occurred after disrupting the interactions that gave rise to the major force peaks in the constant-velocity SMD simulations, confirming that these interactions provided the major barrier to unbending. In most cases, the interactions at both the hybrid/ βTD and the hybrid/EGF4 interfaces were disrupted simultaneously. In the 146 and 97 pN constant-force simulations, however, the interactions at the hybrid/ βTD interface were disrupted first, resulting in an initial

slow-increase phase in the head-tail distance until the interactions at the hybrid/EGF4 interface were also broken. In the 122 pN constant-force simulation, the unbending process was slowed down in the middle of the conformational transition because of the interactions at the knees between the EGF1 and EGF2 domains and between the calf-1 and calf-2 domains. Interestingly, during the simulation with the lowest force of 97 pN, an intermediate state was observed, manifesting as a short plateau with a head-tail distance of ~ 12 nm (Fig. 6A, rightward arrow). In the interme-

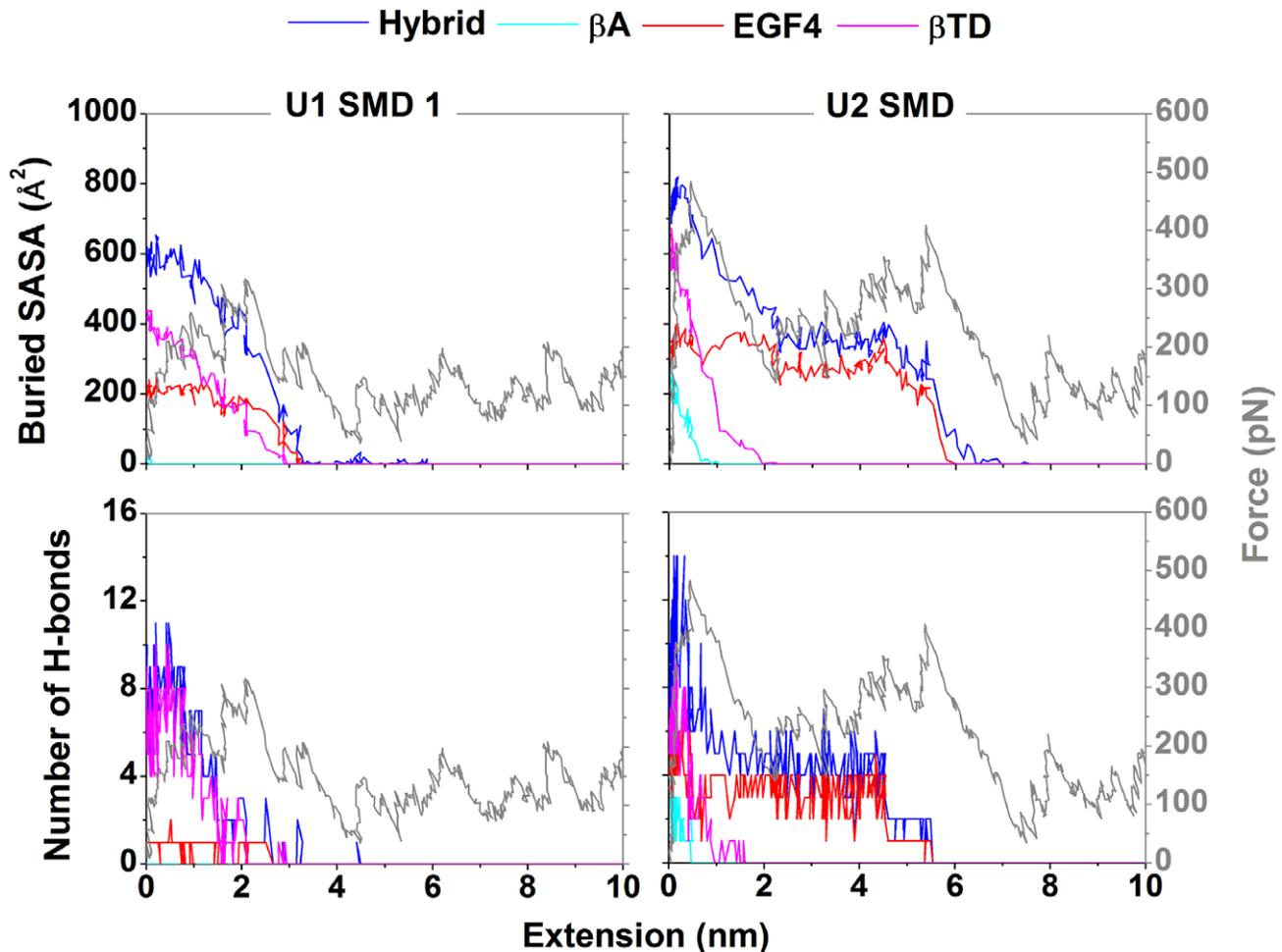


Figure 3. Changes in headpiece-tailpiece interactions near the major force peaks. Buried SASAs (upper row, left ordinate) and numbers of H-bonds (lower row, left ordinate) of the hybrid (blue), β A (cyan), EGF4 (red), and β TD (magenta) domains as well as pulling force (gray, both rows, right ordinate) were plotted vs. extensions for the U1 SMD 1 (left column) and U2 SMD (right column). Some of the curves were obscured due to overlapping.

doi:10.1371/journal.pcbi.1001086.g003

diate state the interactions at both the hybrid/ β TD and hybrid/EGF4 interfaces were disrupted, but the interactions near the knees were still held.

Modeling integrin unbending as a rapid transition between two stable states separated by a barrier, the transition rate constant should be inversely proportional to the time required to overcome the major barrier. For the five U1 simulations, it is evident that this waiting time is shortened by increasing force (Fig. 6A, downward arrows), demonstrating that force accelerates unbending. This is consistent with the Bell model, which assumes that force lowers the barrier to exponentiate the transition rate [26]. Indeed, a plot of the natural log of the waiting time ($\ln t$) vs. pulling force (F) appeared as a straight line (Fig. 6B) well-fitted by the Bell equation [26], $t = t_0 \exp(-F\Delta x/k_B T)$, where $t_0 = 728 \pm 539$ ns is the waiting time at zero force and $\Delta x = 1.2 \pm 0.2$ Å is the width of the energy well that kinetically traps the integrin in the bent conformation. A similar head-tail distance vs. simulation time curve was obtained for the U2 simulation at 195 pN, although a longer waiting time was required to overcome the major barrier than the U1 simulation with the same force (Fig. 6). Taking at the face value, the t_0 value suggests that integrin $\alpha_v\beta_3$ could spontaneously overcome the major barrier to unbending on a time scale of 1 μ s simply by thermally-excited Brownian motions.

Stabilities of different conformations along the unbending pathway

We performed two sets of free dynamics to examine the stabilities of integrin conformations along the unbending pathway after overcoming the major barrier. The first set studied a partially-extended conformation obtained right after the major force peak. Two structures from the respective trajectories of the U1 SMD 1 and U2 SMD 2 at ~ 5 nm extensions were selected as starting structures for free MD 1 & 2, respectively (Fig. 2F). In the free MD simulations, the force at the β A domain was turned off. The constraint at the β TD was released in the free MD 1 but maintained in the free MD 2. In both simulations, the integrin gradually bent back (Fig. 7A and Video S3) as indicated by the decreased C α RMSD relative to the equilibrated bent conformation and the reduced head-tail extension (Fig. 7B). This is particularly evident in the free MD 1 where the C α RMSD dropped to ~ 4 Å within 21 ns and the integrin returned nearly completely to its bent conformation. Not only did the overall structure bend back, but some important interactions between the headpiece and tailpiece that were broken during the simulated unbending were also recovered. Two groups of interactions, including the polar interactions between the hybrid domain and

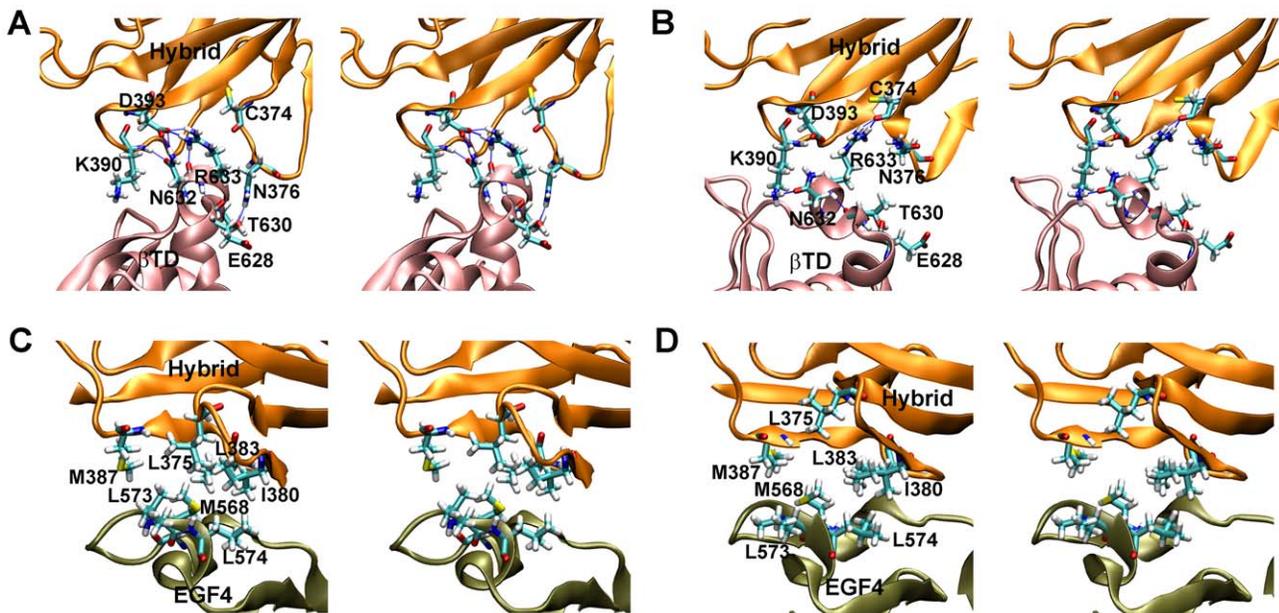


Figure 4. Interactions at hybrid/ β TD and hybrid/EGF4 interfaces. **A & B.** Stereoviews of the post-equilibrated structures of U1 (**A**) and U2 (**B**) at the hybrid/ β TD interface. **C & D.** Stereoviews of the post-equilibrated structures of U1 (**C**) and U2 (**D**) at the hybrid/EGF4 interface. Critical residues are shown as sticks. H-bonds are indicated by dashed lines. The hybrid, β TD, and EGF4 domains are colored in orange, pink, and tan, respectively. doi:10.1371/journal.pcbi.1001086.g004

β TD and the nonpolar interactions between the hybrid and EGF4 domains, were gauged by the respective distances between the center of mass (COM) of the two sidechain oxygen atoms of Asp393 and the COM of the three sidechain nitrogen atoms of Arg633 and between the COM of the sidechains of Leu375, Ile380, and Leu383 and the COM of the sidechains of Met568, Leu573, and Leu574. These two distances were reduced when the integrin bent back (Fig. 7C). In free MD 1, the distance of the nonpolar interactions suddenly dropped to ~ 4 Å and persisted to the end of the simulation, indicating that the nonpolar interactions between the hybrid and EGF4 domains were recovered. These results demonstrated again the importance of the nonpolar interactions in stabilizing the bent conformation. By comparison, the polar interactions were not recovered in the simulations because the Asp393-Arg633 distance was still much larger than that in the bent integrin (Fig. 7C).

The second set of stability analyses was performed on a fully-extended conformation. Two simulations, free MD 3 & 4, were run with their starting structures selected from the trajectories of the U1 SMD 1 & 2, respectively, at ~ 16 nm extensions (Fig. 2F). Free MD began after turning off the pulling force on the β A domain. The constraint at the β TD was released in the free MD 3 but maintained in the free MD 4. In both simulations, the integrin was relaxed and slightly bent back, but remained in a globally extended conformation for >20 ns (Fig. 8A and Video S4). Both C α RMSDs measured from the equilibrated bent conformation and from the starting extended conformation reached plateaus after ~ 5 ns (Fig. 8B). Interestingly, in both simulations, Asp457 of the thigh domain moved to coordinate with the Ca²⁺ ion at the genu of the α_V subunit (Fig. 8C), as observed by a sudden drop in the distance between the COM of the two Asp457 sidechain oxygens and this Ca²⁺ ion to <4 Å at ~ 3 or ~ 18 ns, respectively, which persisted throughout the remaining simulations (Fig. 8E), indicating the stability of the new coordination once it was formed. It should be noted that in the bent conformation, Asp457 was too far away (~ 14 Å) to coordinate with the α_V -genu Ca²⁺ (Fig. 8D).

Only after integrin extension was it physically possible to interact with the α_V -genu Ca²⁺. These results suggest a role for this newly-formed coordination involving Asp457 in stabilizing the extended conformation.

Unbending of liganded integrin $\alpha_V\beta_3$ by pulling its bound cyclic RGD ligand

We next performed constant-velocity SMD simulations to unbend the liganded integrin $\alpha_V\beta_3$ (L1 or L2) by pulling its bound cyclic RGD ligand away from the constrained β TD domain (Fig. 9A). In the L1 SMD 1 and L2 SMD, the integrin readily unbent with the ligand remained bound within 10 ns (Fig. 9A and Video S5 & S6). Compared to the unliganded integrin, the liganded integrin also reached a fully extended conformation with a closed headpiece, but the legs showed a greater degree of relative rotation.

In the initial structure, the RGD peptide interacted with integrin $\alpha_V\beta_3$ via the ligand Asp sidechain oxygen coordinating with the metal ion in the β A domain metal ion-dependent adhesion site (MIDAS) and via the ligand Arg sidechain nitrogen forming a bifurcate H-bond with the Asp218 sidechain oxygen of the α_V β -propeller domain (Fig. 9A). The ligand Asp-MIDAS interaction remained intact throughout both simulations for L1 and L2, as indicated by the ~ 3 Å stable distance between the COM of the two ligand Asp sidechain oxygens and the MIDAS (Fig. 9B). By comparison, the bifurcate ligand Arg-Asp218 H-bond was intact in the L2 SMD simulation (<4 Å stable distance between the COM of the three ligand Arg sidechain nitrogens and the COM of the two Asp218 sidechain oxygens throughout the simulation) but was disrupted in the L1 SMD 1 simulation. Nevertheless, the successful unbending of integrin $\alpha_V\beta_3$ by force applied via a bound ligand suggests that the ligand-integrin $\alpha_V\beta_3$ interaction is stronger than the interaction between the integrin headpiece and tailpiece.

The force-extension curves of the SMD simulations of L1 and L2 displayed a major force peak similar to that observed in the

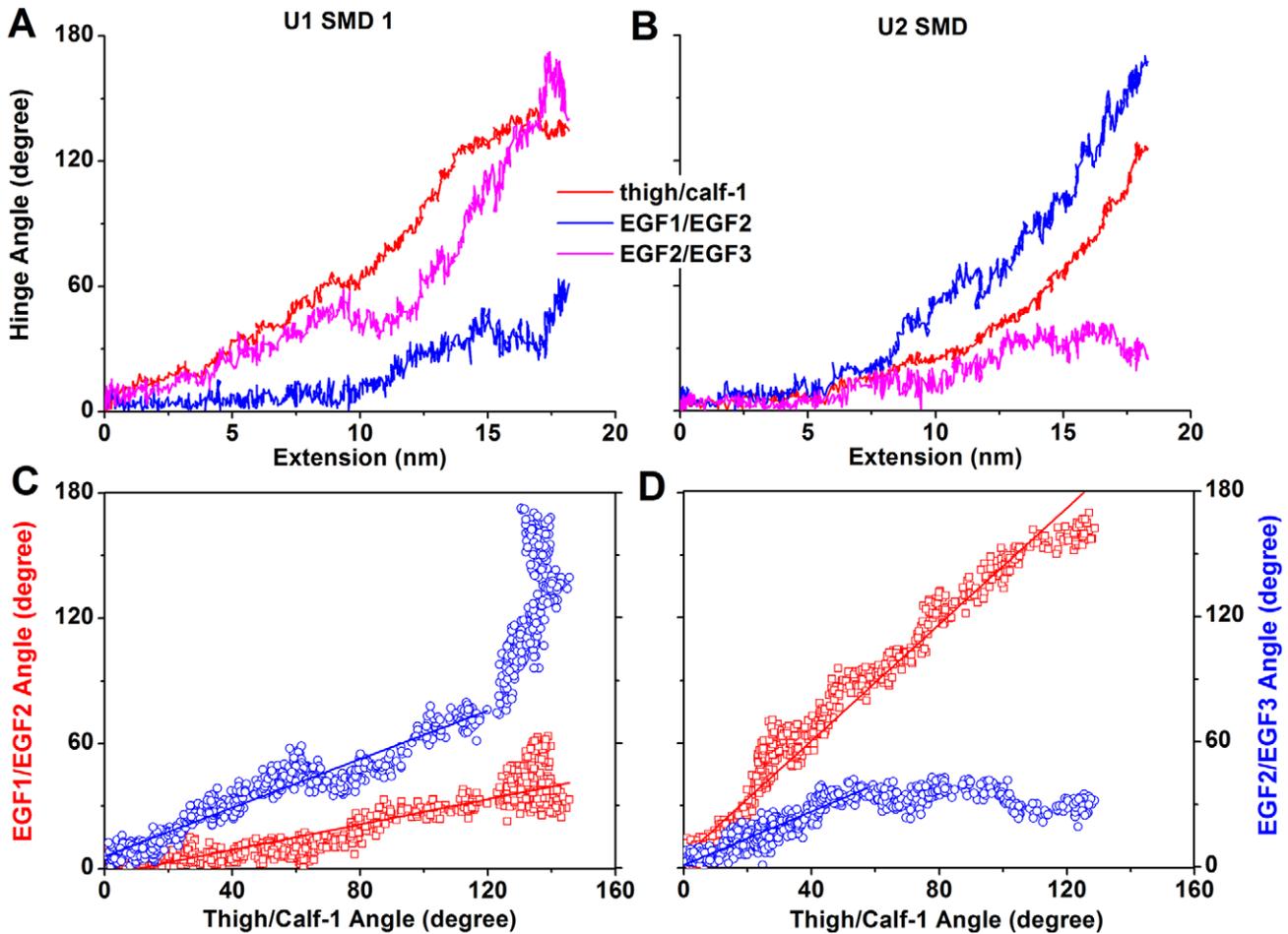


Figure 5. Changes in hinge angles at the α/β knees during unbending. **A & B.** Time courses of thigh/calf-1 (red), EGF1/EGF2 (blue), and EGF2/EGF3 (pink) hinge angles in the U1 SMD 1 (**A**) and U2 SMD (**B**). **C & D.** The EGF1/EGF2 (red squares) and EGF2/EGF3 (blue circles) hinge angles are plotted against the thigh/calf-1 hinge angle for the U1 SMD 1 (**C**) and U2 SMD (**D**). Solid lines are fits to the linear regions.
 doi:10.1371/journal.pcbi.1001086.g005

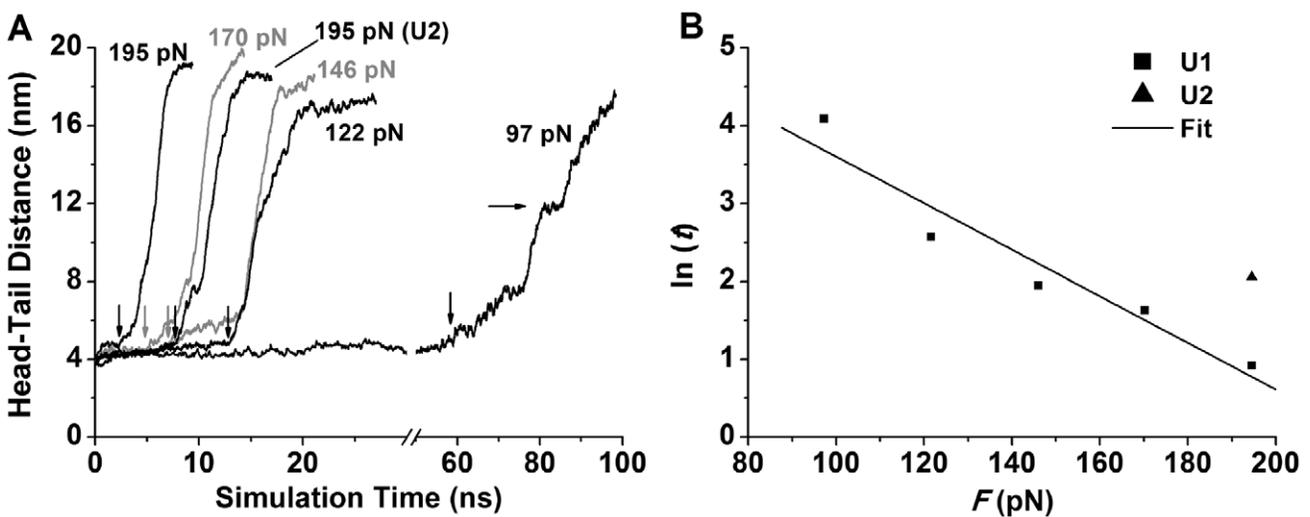


Figure 6. Constant-force SMD simulations. **A.** Head-tail distances vs. time of constant-force SMD simulations with the indicated forces. One simulation for U2 is indicated in parentheses and the others are for U1. Downward arrows indicate the moments when unbending started. A rightward arrow indicates an intermediate state. **B.** Natural log of waiting time t (in ns) for unbending vs. force data (symbols) and the Bell model fit (line) to the U1 data.
 doi:10.1371/journal.pcbi.1001086.g006

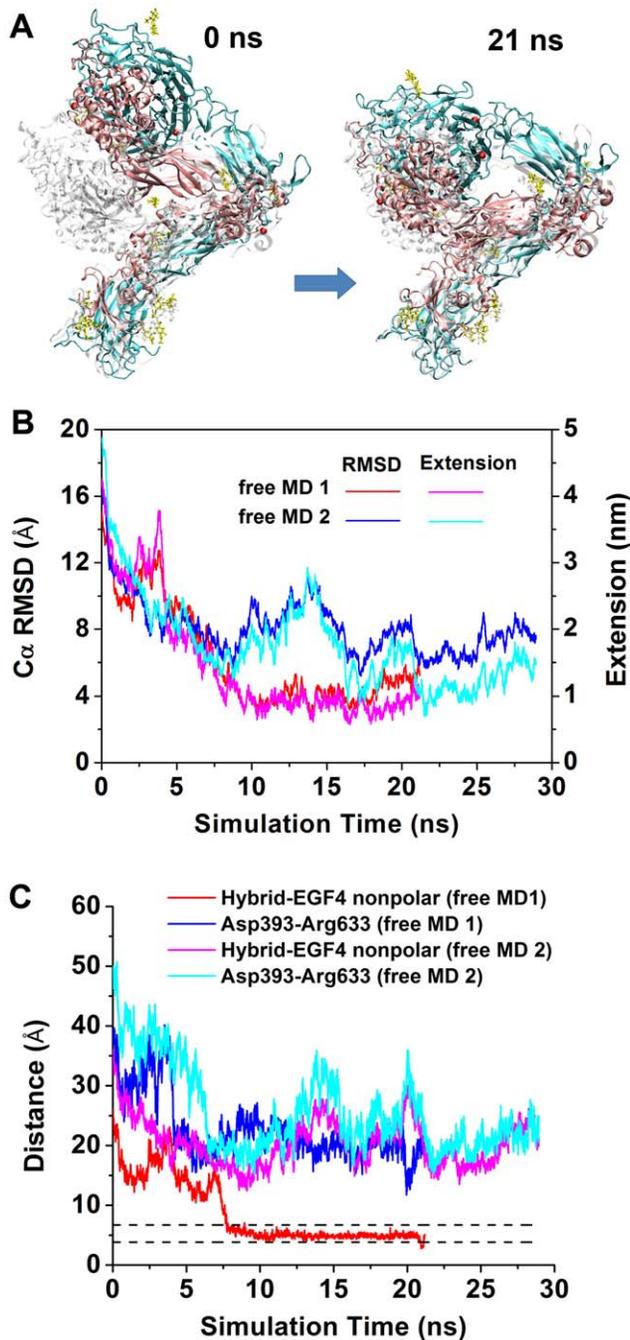


Figure 7. Free MD simulations of a partially-extended conformation. **A.** Snapshots of the U1 free MD 1 at indicated times showing rebending from a partially-extended integrin (colored) to the equilibrated bent conformation (gray). **B.** Time courses of $C\alpha$ RMSDs relative to the equilibrated bent structure (red and blue, left ordinate) and head-tail extensions (magenta and cyan, right ordinate) in the U1 free MD 1 (red and magenta) and 2 (blue and cyan). **C.** Distances between the interacting residues, the nonpolar group (red and magenta) and the Asp393-Arg633 salt bridge (blue and cyan) at the respective hybrid/ β TD and hybrid/EGF4 interfaces vs. simulation time of the U1 free MD 1 (red and blue) and 2 (magenta and cyan). As references, the upper and lower dashed lines indicate the respective distances of the nonpolar group and the Asp393-Arg633 salt bridge for the equilibrated bent U1 structure.

doi:10.1371/journal.pcbi.1001086.g007

SMD simulations of U1 and U2 (Fig. 9C). Additionally, we observed two smaller peaks in the L1 SMD 1 and one smaller peak in the L2 SMD. Inspection of the changes of buried SASAs between the headpiece and tailpiece of integrin $\alpha_V\beta_3$ revealed that the second peak in the L1 SMD 1 was due to interactions between the hybrid and EGF3 domains while the third peak in the L1 SMD 1 and the second peak in the L2 SMD were both due to interactions at the α/β knees (Fig. S5). Finally, we performed one more constant-velocity SMD simulation on L1 (L1 SMD 2) by pulling the same β A domain as in the SMD simulations of U1 and U2 (instead of pulling on the RGD ligand as in the L1 SMD 1 and L2 SMD). This time only the first peak was seen on the force-extension curve (Fig. 9C). These results suggest that the force direction plays a role in the determination of the unbending pathway after the first major force peak.

To examine the stability of the liganded integrin after extension, we performed two free MD simulations for the final structures of the L1 SMD 1 and L2 SMD but did not observe the formation of the α_V Asp457-Mg²⁺ coordination at the α -knee (Ca²⁺ in the unliganded integrin was replaced by Mg²⁺ in the liganded integrin). This may be due to the different post-equilibration structures of the unliganded and liganded integrins. Despite that the β A domain was pulled the same way in the L1 SMD 2 as the previous simulations of the unliganded integrin, the α_V Asp457 was far away from the α -knee Mg²⁺ in the resulting extended liganded integrin. By comparison, the α_V Asp457 was very close to the α -knee Ca²⁺ in the unliganded integrin after extension even before further equilibration. We note that without the α_V Asp457/ α -knee Mg²⁺ coordination, the α -knee tended to rebend because the thigh/calf-1 hinge angle decreased significantly in one of the two free dynamics simulations of the liganded integrin (L1 free MD) (Fig. S6). With the α_V Asp457/ α -knee Ca²⁺ coordination, by comparison, the thigh/calf-1 hinge angle remained stable at certain levels in the two free dynamics simulations of the extended unliganded integrin (U1 free MD 3 & 4). The differential stabilities of the α -knee in the absence and presence of the α_V Asp457/ α -knee metal ion coordination supports the assertion that this metal ion coordination stabilizes, at least partly, the extended conformation.

Discussion

X-ray crystallographic [4–10], electron microscopic [11–13], and antibody epitope mapping [27] studies have shown different static conformations of integrins corresponding to their different affinity states. The MD simulations reported here have connected the static conformations with dynamic processes, added time and force information, and provided structural insights to the continuous conformational changes of the integrin $\alpha_V\beta_3$ ectodomain. Our results suggest that tensile forces applied to either the β A and/or β -propeller domains (Fig. 2) or the bound cyclic RGD ligand (Fig. 9) can easily induce the change of integrin $\alpha_V\beta_3$ from a bent to an extended conformation. This work represents the first study in which the dynamic process of unbending of a complete integrin ectodomain was simulated in atomic details. Because no major distortions of individual domains resulted from pulling, our simulated structures of extended integrins should be more accurate than models obtained by simply rotating the bent crystal structures at the knees [8] or fitting various domains from the bent crystal structures into low resolution EM images of extended integrins [28]. Furthermore, that force can easily extend an integrin suggests an intriguing possible mechanism of force-induced integrin activation. Indeed, shear stress applied to lymphocytes promotes robust integrin-mediated adhesion [16]. In addition, either

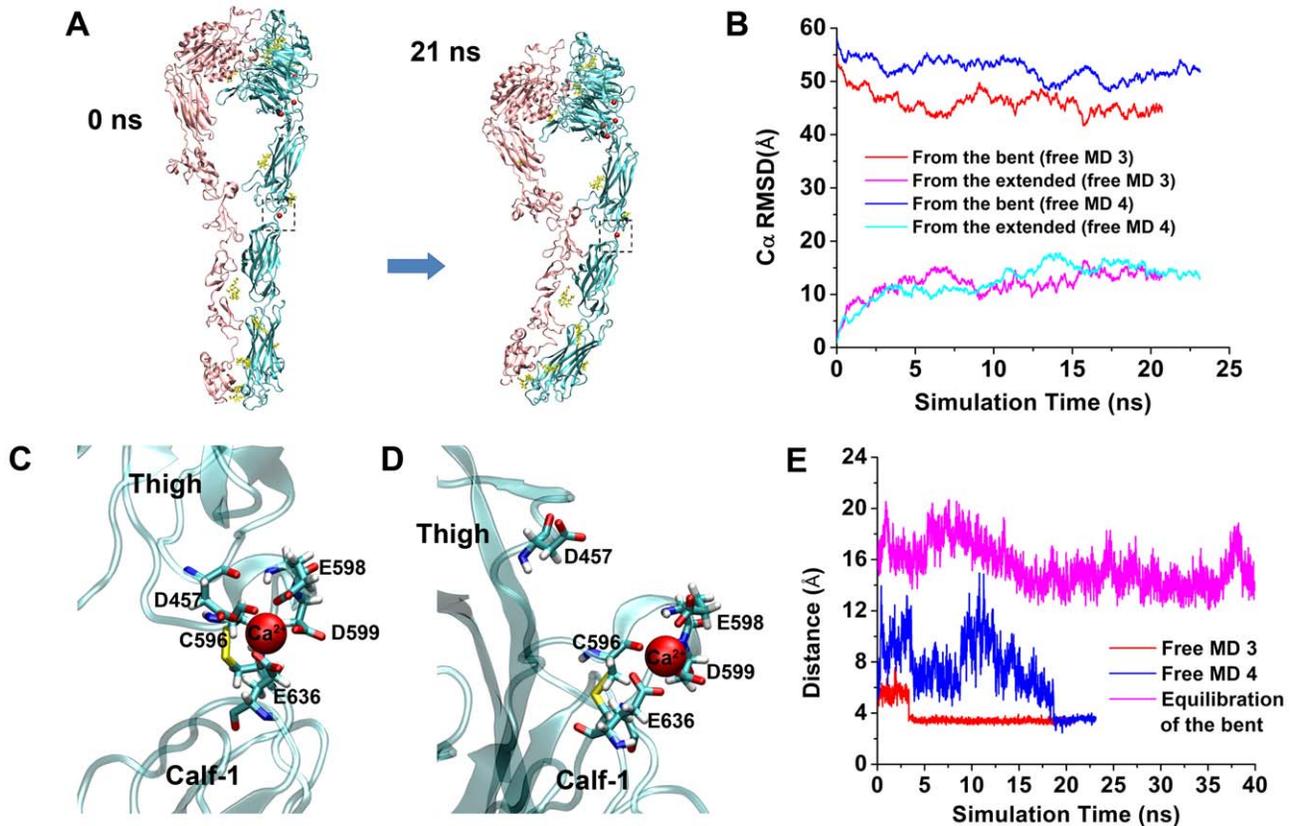


Figure 8. Free MD simulations of a fully-extended conformation. **A.** Snapshots of the U1 free MD 3 at indicated times showing the relaxation of a fully-extended integrin. Dashed boxes indicated the location of the α -knee Ca^{2+} . **B.** Time courses of $\text{C}\alpha$ RMSDs relative to the equilibrated bent structure (red and blue) or the starting fully-extended structure (magenta and cyan) in the U1 free MD 3 (red and magenta) and 4 (blue and cyan). **C & D.** Metal-ion coordination at the α -knee of the extended U1 at the end of the free MD 3 (**C**) or the bent U1 at the end of equilibration (**D**). Sticks represent residues and the red sphere represents the α -knee Ca^{2+} . **E.** Time courses of distances between Asp457 of the α_v subunit and the α -knee Ca^{2+} in the U1 free MD 3 (red), the U1 free MD 4 (blue), and the equilibration of the bent U1 (magenta). doi:10.1371/journal.pcbi.1001086.g008

intracellular force by the cytoskeleton or extracellular force by shear strengthens adhesions mediated by integrin $\alpha_5\beta_1$ -fibronectin bonds [17]. Moreover, recent single-bond experiments have demonstrated catch bond behavior (such that force prolongs bond lifetime) for bonds between integrin $\alpha_5\beta_1$ and fibronectin [18] and between integrin $\alpha_L\beta_2$ and intercellular adhesion molecule 1 [19].

Although tensile forces readily unbent integrin $\alpha_v\beta_3$, we did not observe hybrid domain swing-out, a key conformational change in models of integrin activation [10,11], in the SMD simulations (Figs. 2 and 9) or free dynamics simulations of the extended integrin with closed legs (Fig. 8). This result differs from previous SMD simulations on the $\alpha_v\beta_3$ headpiece [20,21], where pulling the ligand binding site at the β_A domain and the hybrid domain C-terminus induced the hybrid domain to swing out. Intuitively, when tensile forces apply to the V-shape $\alpha_v\beta_3$ headpiece, the hybrid domain would naturally swing out to open the headpiece. Pulling the whole ectodomain would be quite different. In the SMD simulations of an extended model of $\alpha_{IIb}\beta_3$, a lateral force opened the closed α/β legs and induced the hybrid domain to swing out, but an axial force pulling along the straight integrin kept the hybrid domain closed [8]. In our SMD simulations with only axial forces, the legs remained closed and the hybrid domain did not swing out. It is not clear whether axial and lateral forces would apply to integrins simultaneously or sequentially under physiological situations. However, we observed extensive contacts between the two α/β legs that were stronger than those between

the headpiece and tailpiece (data not shown), suggesting that opening the closed legs may cost higher energy than unbending. Therefore, different forces may be required to first unbend an integrin and then open the legs and the hybrid domain. There may be mechanisms other than unbending and hybrid domain swing-out for force to increase binding affinity and/or bond lifetime of integrins with ligands. Indeed, lifetimes of $\alpha_5\beta_1$ -fibronectin [18] and $\alpha_L\beta_2$ -intercellular adhesion molecule 1 [19] bonds have been observed to be prolonged by axial instead of lateral forces regardless of whether the integrins were unbent (and/or the hybrid domain was swung out) by force or the integrins had already been extended (and/or the hybrid domain had already been swung out) prior to the application of force.

We identified two groups of critical interactions between the headpiece and tailpiece of the β_3 subunit (Fig. 4) that form the major energy barrier to the unbending of integrin $\alpha_v\beta_3$. One group mainly consists of polar interactions between the hybrid domain and the βTD , including several H-bonds and one salt bridge between Asp393 and Arg633. Indeed, Arg633 has been identified as a key residue to keep integrin $\alpha_v\beta_3$ in the bent conformation by NMA [24]. To verify the importance of Arg633, the authors further showed experimentally that its deletion or substitution by Ala enhanced $\alpha_{IIb}\beta_3$ -fibrinogen binding. The other group of critical interactions includes hydrophobic interactions between the hybrid and EGF4 domains. Not only did these interactions contribute to the major force peak resisting unbend-

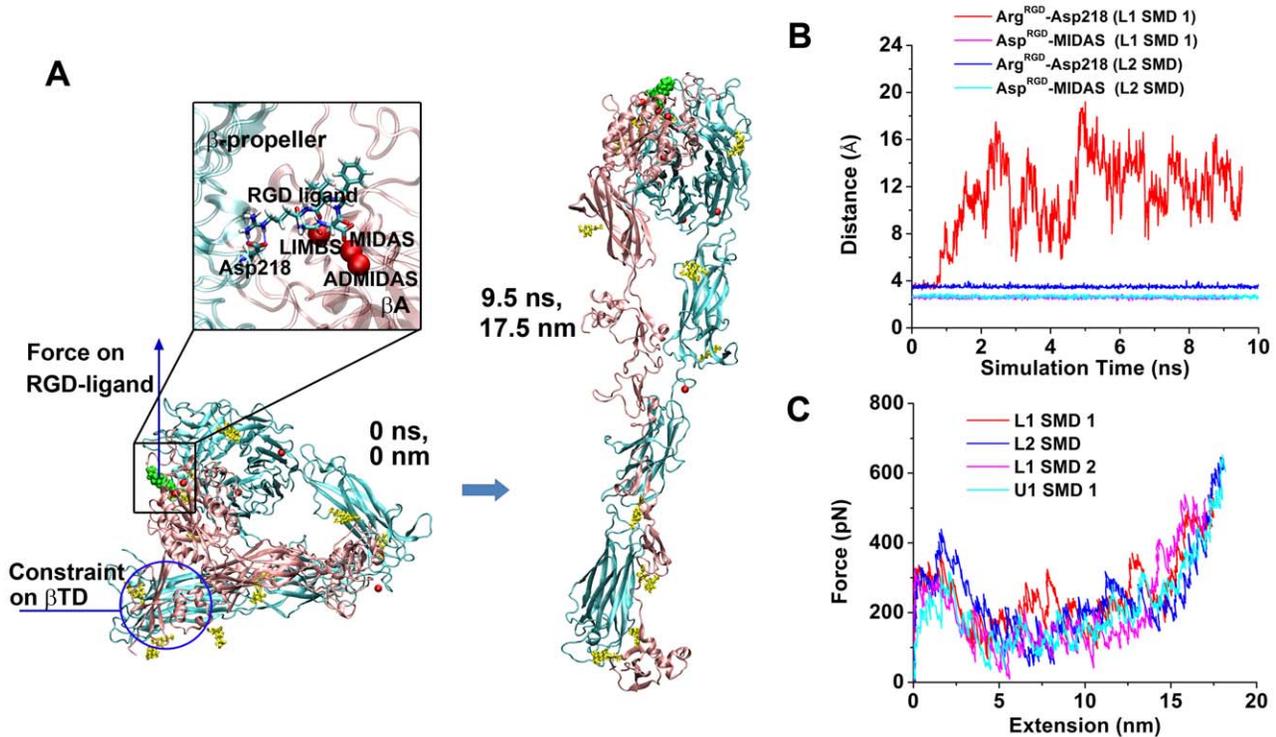


Figure 9. Forced unbending of liganded integrin $\alpha_v\beta_3$. **A.** Snapshots of a liganded integrin $\alpha_v\beta_3$ in the bent and fully-extended conformations at the indicated times and extensions in the L1 SMD 1. The β TD was constrained as shown by a circle. The RGD ligand (green spheres, same color coding and representations in all figures and videos) where force was loaded was zoomed-in to show the ligand binding site with a different orientation for better display, where the RGD ligand is shown as sticks and three Mg^{2+} ions as red spheres. LIMBS, ligand-associated metal binding site; ADMIDAS, adjacent to MIDAS. **B.** Time courses of distances between the ligand Arg and the α_v Asp218 (red and blue) or between the ligand Asp and the α_v MIDAS Mg^{2+} (magenta and cyan) in the L1 SMD 1 (red and magenta) and L2 SMD (blue and cyan). Some of the curves were obscured due to overlapping. **C.** Force-extension curves for the indicated SMD simulations. The U1 SMD 1 curve was replotted for comparison. doi:10.1371/journal.pcbi.1001086.g009

ing, but they were also seen to reform during rebending of the partially-extended integrin (Fig. 7). These results predict that disrupting the hydrophobic interactions by mutating the residues involved, including Leu375, Ile380, Leu383, Met387, Met568, Leu573, and Leu574, to polar residues will promote extension of β_3 integrins. Besides the two groups of interactions identified from our simulations, there may be other interactions that play roles in the conformational changes of integrins. Indeed, interactions between a β hairpin protruding from the β -propeller domain and a region in the middle of the EGF3 and EGF4 domains have been shown as a clasp in restraining integrin activation [29]. This is consistent with our simulations showing that these interactions were maintained until the integrin was unbent.

Our constant-force SMD simulations indicate that the time required to overcome the major barrier to unbending follows the Bell model [26] (Fig. 6). The value of $\Delta x = 1.2 \pm 0.2$ Å suggests a narrow energy well not very sensitive to force. The extrapolated zero-force waiting time of $t_0 = 728 \pm 539$ ns suggests that the major barrier could be spontaneously overcome very rapidly on a time scale of 1 μ s, allowing the integrin to reach a partially-extended conformation. It should be noted that these results are based on one simulation per force only, so the inferred zero-force waiting time may not be accurate. We also cannot exclude the possibility of a different unbending time-force relationship at lower forces. On the other hand, our free MD simulations suggested that the partially-extended integrin could bend back on a much shorter time scale of 10 ns (Fig. 7), so the rebending rate may be much faster than the unbending rate. Therefore, although unbending

may occur spontaneously, the integrin may still far more likely assume the bent conformation at zero force. It may also undergo fast transitions between the bent and partially-extended conformation like “breathing”. Springer and coworkers propose that during integrin conformation “breathing”, epitopes on the β -leg may expose for antibody binding [11,14]. The binding of an antibody acts as a wedge to keep the interface between the headpiece and tailpiece open, which stabilizes the extended conformation and thus activates integrins. Indeed, EM studies observe that a small group of integrin $\alpha_v\beta_3$ under inactive conditions has a wider separation between the headpiece and tailpiece while the majority exhibits headpiece-tailpiece contacts [11]. Upon stimulations, the conformational equilibrium in a population of integrins may readily shift so that the extended conformation becomes more popular.

Another interesting observation is the formation of a new coordination between the thigh domain Asp457 and the metal ion at the α -genu when the unliganded integrin became fully extended (Fig. 8), although this was not observed in the unbending simulations of the liganded integrin probably due to the different starting structure and insufficient simulation time. Because the new coordination was very stable once it was formed (Fig. 8E) and the α -knee tended to rebend when the new coordination was not formed (Fig. S6), the new coordination likely plays a role in stabilizing the extended conformation. In addition, both Asp457 and the α -genu metal ion site are conserved across species (Fig. S7A), suggesting a functional role. While future mutagenesis experiments are required to provide definitive tests, the putative

coordination between Asp457 and the α -genu metal ion upon integrin extension may explain why the majority of $\alpha_V\beta_3$ integrins adopt bent conformations in Ca^{2+} but extended conformations in Mn^{2+} [11]. The explanation assumes different propensities for distinct metal ions to coordinate with Asp457 such that distinct metal ion conditions favor different fractions of bent vs. extended integrins. It should be noted that among all 18 known human α subunits, residue 457 has wide variations, although the α -genu metal ion site is largely conserved (Fig. S7B). Only in several α subunits, including α_5 , α_7 , and α_8 , is Asp457 conservatively substituted by Glu. Therefore, the putative Asp457/ α -genu metal ion coordination is likely a specific property for a subset of integrins.

It remains debatable whether the deadbolt or switchblade model describes the mechanism of integrin activation [2]. Our simulations may seem to favor the switchblade model because force induces a switchblade-like extension. However, initial ligand binding before force loading could be regulated by a “deadbolt”. Future experimental and computational studies are needed to clarify the mechanism of integrin activation.

Methods

System setup

Four systems were set up for MD simulations: U1, U2, L1, and L2 (Table S1). U1 was modeled after the early crystal structure of the unliganded integrin $\alpha_V\beta_3$ ectodomain (PDB code 1U8C) [6] available at the time when we started this study, in which the EGF1 and EGF2 domains at the genu of the β_3 subunit were unresolved. To complete the ectodomain, we used MODELLER [30] to build a homology model for the two missing domains based on the crystal structure of a fragment of the β_2 subunit (PDB code 2P28) [31] and used TMD to fit it to the crystal structure (Text S1 and Fig. S8). The modeled EGF1 and EGF2 domains plus the PSI domain from the 1U8C structure were then added to the liganded integrin $\alpha_V\beta_3$ ectodomain (PDB code 1L5G) [5] to obtain L1. U2 is the recently released crystal structure of the unliganded integrin $\alpha_V\beta_3$ ectodomain plus a short α/β transmembrane fragment, where the EGF1 and EGF2 domains are visible (PDB code 3IJE) [7]. Wherever resolvable, the 1U8C structure is very close to the 3IJE structure. Our homology model of the EGF1 and EGF2 domains are similar to those of the 3IJE structure in orientation and majority of the tertiary structures, with noticeable variations only in the loops and the linker between the two domains (Fig. S4). L2 was obtained by extracting the EGF1, EGF2, and PSI domains from the 3IJE structure and adding them to the 1L5G structure. Therefore, U1 and U2 are highly comparable except for the EGF1 and EGF2 domains; so are L1 and L2. For L1 and L2, we replaced nonstandard N-Methylvaline and D-form Phenylalanine in the cyclic-RGD ligand to standard Valine and L-form Phenylalanine, respectively. We also replaced Mn^{2+} ions with Mg^{2+} because force field parameters for Mn^{2+} were not available.

We employed LEaP in AMBER8 package [32] to prepare solvated structures with TIP3P [33] water boxes (Fig. 1B). The closest distance between the walls of the water boxes and the proteins was 15 Å while the closest distance between water molecules and proteins was set to 1 Å. Four water boxes with different dimensions were set up for the four structures (Table S1). Na^+ and Cl^- ions were added to neutralize the systems at a 150 mM salt concentration. After equilibration, the water boxes were further enlarged for SMD simulations (Fig. 2A) and more Na^+ and Cl^- ions were added accordingly to maintain the 150 mM salt concentration.

MD simulations

MD simulations were performed using NAMD [34]. Duan et al. [35] and GLYCAM04/06 [36,37] force fields were used for amino acids and carbohydrates attached to the proteins, respectively. We used 2 fs time step, 12 Å cutoff for non-bonded force, and 10 Å switching distance for smoothing functions of non-bonded force. Bonds involving hydrogen were set rigid by using the SHAKE algorithm [38] for protein and the SETTLE algorithm [39] for water. Periodic boundary conditions were applied and the Particle Mesh Ewald method [40] was used to calculate full electrostatic interactions every 4 fs. Atomic coordinates of the systems were saved every 1 ps.

First, each system was energy-minimized for three consecutive 10,000 conjugate-gradient steps: first with all protein atoms fixed, second with only the backbone atoms fixed, and third with all atoms free. Then, the systems were gradually heated from 0 to 300 K in 120 ps with constraints of $1 \text{ kcal mol}^{-1} \text{ \AA}^{-2}$ spring constants applied on all protein atoms under constant volume. Next, pressure was adjusted to 1 atm in 100 ps with the Langevin piston method [41] under constant temperature controlled with Langevin dynamics. After that, the constraints on the protein atoms were gradually released in 100 ps under constant volume and constant temperature (NVT). Finally, 40 (or 50) ns equilibrations were performed for U1 and L1 (or U2 and L2) under constant pressure and constant temperature (NPT). The pressure was maintained at 1 atm by the Langevin piston method while the temperature was maintained at 300 K by Langevin dynamics with a damping coefficient of 5 ps^{-1} .

After equilibration in the small water boxes (cf. Fig. 1B), more water molecules were added to enlarge the water boxes (cf. Fig. 2A). For equilibration of the enlarged water boxes, the systems were first energy-minimized for 10,000 conjugate-gradient steps with all protein atoms fixed, next heated from 0 to 300 K in 120 ps with spring constraints of $1 \text{ kcal mol}^{-1} \text{ \AA}^{-2}$ spring constant on all protein atoms under constant volume followed by 2–4 ns equilibration in NPT ensembles, then set free by gradually releasing constraints on the protein atoms in 100–400 ps followed by 2–4 ns final equilibration in NPT ensembles. The enlarged systems were then ready for SMD simulations. In all production SMD and free MD simulations, the controls on pressure and temperature were turned off so as to reduce disturbance on the dynamics.

In SMD simulations, a group of C α atoms were selected. Then force or constraint was exerted on the COM of the selected atoms. When different domains were pulled or constrained, the residues were selected as follows: β A residues 113–117, 151–156, 190–197, 244–250, 306–310, and 329–332; β -propeller residues 22–26, 97–101, 160–164, 225–229, 279–283, 343–347, and 407–411; β TD residues 610–620, 639–642, 656–658, 665–670, and 679–682; and all five residues of the cyclic RGD ligand. While force was on the pulling COM, a harmonic potential with a spring constant of $10 \text{ kcal mol}^{-1} \text{ \AA}^{-2}$ was added to the constraint COM. In the constant-velocity SMD simulations [25], the pulling COM was harmonically constrained with a force, $F = k(vt - x)$, where k is the spring constant, v is the pulling velocity, t is time, and x is the coordinate along the force direction. A total of ~ 468 ns production simulations were performed, including 8 constant-velocity and 5 constant-force SMD simulations for U1, 1 constant-velocity and 1 constant-force SMD for U2, 2 constant-velocity SMD for L1, 1 constant-velocity SMD for L2, 4 free MD for U1, 1 free MD for L1, and 1 free MD for L2 (Table S1).

Analysis of MD trajectories

VMD [42] was employed to analyze simulations, render molecular graphics, and generate trajectory videos. SASA was calculated with 1.4 Å probe radius. Buried SASA between two contacting portions was calculated as the difference between the SASAs of one portion without and with the other portion. Restricted to one domain during SASA calculation, the buried SASA of that domain was obtained. An H-bond was defined by a <3.5 Å donor-acceptor distance and a >120° donor-hydrogen-acceptor angle. Hinge angles were measured using Hingefind [43]. The various $\alpha_V\beta_3$ domains are defined as follows: β -propeller, residues 1–438; thigh, residues 439–600; calf-1, residues 601–738; calf-2, residues 739–956; PSI, residues 1–57; hybrid, residues 58–110 and 354–434; β A, residues 111–353; EGF1, residues 435–472; EGF2, residues 473–522; EGF3, residues 523–559; EGF4, residues 560–599; β -ankle, residues 600–605; β TD, residues 606–690.

Supporting Information

Figure S1 Changes in headpiece-tailpiece interactions near the major force peaks. Buried SASAs (upper row, left ordinate) and numbers of H-bonds (lower row, left ordinate) of hybrid (blue), β A (cyan), EGF4 (red), and β TD (magenta) domains as well as pulling force (gray, both rows, right ordinate) were plotted vs. extensions for the U1 SMD 2 (left column) and U1 SMD 3 (right column). Some of the curves were obscured due to overlapping.
Found at: doi:10.1371/journal.pcbi.1001086.s001 (0.45 MB TIF)

Figure S2 H-bonds at the hybrid/EGF4 interface of U2. Stereoview of the post-equilibrated U2 structure at the interface between hybrid (orange) and EGF4 (tan) with residues involved in H-bonds (indicated by dashed lines) shown as sticks.
Found at: doi:10.1371/journal.pcbi.1001086.s002 (1.74 MB TIF)

Figure S3 Changes in hinge angles at the α/β knees during unbending. A & B. Time courses of thigh/calf-1 (red), EGF1/EGF2 (blue), and EGF2/EGF3 (pink) hinge angles in the U1 SMD 2 (A) and 3 (B). C & D. The EGF1/EGF2 (red squares) and EGF2/EGF3 (blue circles) hinge angles are plotted against the thigh/calf-1 hinge angle for the U1 SMD 2 (C) and 3 (D). Solid lines are fits to the linear regions.
Found at: doi:10.1371/journal.pcbi.1001086.s003 (0.50 MB TIF)

Figure S4 Comparison of the homology model of the EGF1 and EGF2 domains with the crystal structure. The homology model (red) and the crystal structure (blue, PDB code 3IJE) were aligned using C α atoms of the β_3 subunit other than the EGF1 and EGF2 domains (left and middle) or using the C α atoms of the EGF1 and EGF2 domains (right).
Found at: doi:10.1371/journal.pcbi.1001086.s004 (3.03 MB TIF)

Figure S5 Buried SASA between the headpiece and tailpiece during unbending of the liganded $\alpha_V\beta_3$. Buried SASAs (colored, left ordinate) of the indicated domains were plotted vs. simulation time along with pulling force (gray, right ordinate) for the L1 SMD 1 and L2 SMD.
Found at: doi:10.1371/journal.pcbi.1001086.s005 (0.47 MB TIF)

Figure S6 Changes of the thigh/calf-1 hinge angle in the free MD simulations of the extended integrin. The thigh/calf-1 hinge angles are plotted against simulation time for the indicated simulations.
Found at: doi:10.1371/journal.pcbi.1001086.s006 (0.14 MB TIF)

Figure S7 Amino acid sequence alignment of the α_V subunit. The sequences were aligned across species (A) or human α family

members (B) by using ClustalW2 [44]. The sequences were retrieved from UniProt Knowledgebase (UniProtKB) [45]. Conserved mutations at residue 457 and the α -genu metal ion site are highlighted. “*” indicates identical residues, “:” indicates conserved substitutions, and “.” indicates semi-conserved substitutions.

Found at: doi:10.1371/journal.pcbi.1001086.s007 (6.59 MB TIF)

Figure S8 Building complete ectodomain models of integrin $\alpha_V\beta_3$. A. Amino acid sequence alignment between β_2 and β_3 in the region containing the PSI, EGF1, and EGF2 domains with ClustalW2 [44]. B. Alignment of the template and the homology model. On the left, the hybrid and EGF3 domains (blue) from the crystal structure of integrin $\alpha_V\beta_3$ (PDB code 1U8C) were aligned to the template (gray) of the β_2 fragment (PDB code 2P28) before homology modeling. On the right, the final homology model (red) was compared to the template. C. Targeting the extended β_3 model (red) to the bent β_3 structure (gray) by TMD simulation. Snapshots were taken at indicated times. D. The final bent β_3 model (red) in the bent $\alpha_V\beta_3$ structure (α_V , yellow; β_3 , gray). E. RMSD relative to the bent structure for all heavy atoms of the PSI, hybrid, and EGF3 domains during the TMD simulation. F. Comparison of the DOPE scores of the homology model and the template.
Found at: doi:10.1371/journal.pcbi.1001086.s008 (5.24 MB TIF)

Table S1 Summary of MD simulations for integrin $\alpha_V\beta_3$.
Found at: doi:10.1371/journal.pcbi.1001086.s009 (0.04 MB DOC)

Text S1 Building complete ectodomain models of unliganded and liganded integrin $\alpha_V\beta_3$.

Found at: doi:10.1371/journal.pcbi.1001086.s010 (0.06 MB DOC)

Video S1 Unbending of unliganded integrin $\alpha_V\beta_3$ in the U1 SMD 1. The β A domain was pulled vertically away from the constrained β TD. The running simulation time is indicated. The α_V subunit is in cyan and the β_3 subunit is in pink. The same color codes are used in all videos.
Found at: doi:10.1371/journal.pcbi.1001086.s011 (4.65 MB AVI)

Video S2 Unbending of unliganded integrin $\alpha_V\beta_3$ in the U2 SMD. The β A domain was pulled vertically away from the constrained β TD.
Found at: doi:10.1371/journal.pcbi.1001086.s012 (4.55 MB AVI)

Video S3 Rebending of partially-extended unliganded integrin $\alpha_V\beta_3$ in the U1 free MD 1. The simulation started from the partially-extended structure that was selected from the U1 SMD 1. Nothing was constrained during the simulation. The bent structure is in gray for comparison.
Found at: doi:10.1371/journal.pcbi.1001086.s013 (9.82 MB AVI)

Video S4 Relaxation of fully-extended unliganded integrin $\alpha_V\beta_3$ in the U1 free MD 3. The simulation started from the fully-extended structure that was selected from the U1 SMD 1. Nothing was constrained during the simulation.
Found at: doi:10.1371/journal.pcbi.1001086.s014 (5.82 MB AVI)

Video S5 Unbending of liganded integrin $\alpha_V\beta_3$ in the L1 SMD 1. The cyclic RGD ligand (green spheres) was pulled vertically away from the constrained β TD.
Found at: doi:10.1371/journal.pcbi.1001086.s015 (4.52 MB AVI)

Video S6 Unbending of liganded integrin $\alpha_V\beta_3$ in the L2 SMD. The cyclic RGD ligand (green spheres) was pulled vertically away from the constrained β TD.
Found at: doi:10.1371/journal.pcbi.1001086.s016 (4.72 MB AVI)

Acknowledgments

We thank Rodger P. McEver for helpful discussions. We also acknowledge NSF TeraGrid for providing supercomputer time via PSC DAC grant TG-MCB070089N and TACC TRAC grant TG-MCA08X014.

References

- Hynes RO (2002) Integrins: bidirectional, allosteric signaling machines. *Cell* 110: 673–687.
- Arnaout MA, Mahalingam B, Xiong JP (2005) Integrin structure, allostery, and bidirectional signaling. *Annu Rev Cell Dev Biol* 21: 381–410.
- Luo BH, Springer TA (2006) Integrin structures and conformational signaling. *Curr Opin Cell Biol* 18: 579–586.
- Xiong JP, Stehle T, Diefenbach B, Zhang R, Dunker R, et al. (2001) Crystal structure of the extracellular segment of integrin $\alpha V\beta 3$. *Science* 294: 339–345.
- Xiong JP, Stehle T, Zhang R, Joachimiak A, Frech M, et al. (2002) Crystal structure of the extracellular segment of integrin $\alpha V\beta 3$ in complex with an Arg-Gly-Asp ligand. *Science* 296: 151–155.
- Xiong JP, Stehle T, Goodman SL, Arnaout MA (2004) A novel adaptation of the integrin PSI domain revealed from its crystal structure. *J Biol Chem* 279: 40252–40254.
- Xiong JP, Mahalingam B, Alonso JL, Borrelli LA, Rui X, et al. (2009) Crystal structure of the complete integrin $\alpha V\beta 3$ ectodomain plus an α/β transmembrane fragment. *J Cell Biol* 186: 589–600.
- Zhu J, Luo BH, Xiao T, Zhang C, Nishida N, et al. (2008) Structure of a complete integrin ectodomain in a physiologic resting state and activation and deactivation by applied forces. *Mol Cell* 32: 849–861.
- Xie C, Zhu J, Chen X, Mi L, Nishida N, et al. (2010) Structure of an integrin with an αI domain, complement receptor type 4. *EMBO J* 29: 666–679.
- Xiao T, Takagi J, Collier BS, Wang JH, Springer TA (2004) Structural basis for allostery in integrins and binding to fibrinogen-mimetic therapeutics. *Nature* 432: 59–67.
- Takagi J, Petre BM, Walz T, Springer TA (2002) Global conformational rearrangements in integrin extracellular domains in outside-in and inside-out signaling. *Cell* 110: 599–511.
- Takagi J, Strokovich K, Springer TA, Walz T (2003) Structure of integrin $\alpha 5\beta 1$ in complex with fibronectin. *EMBO J* 22: 4607–4615.
- Nishida N, Xie C, Shimaoka M, Cheng Y, Walz T, et al. (2006) Activation of leukocyte $\beta 2$ integrins by conversion from bent to extended conformations. *Immunity* 25: 583–594.
- Beglova N, Blacklow SC, Takagi J, Springer TA (2002) Cysteine-rich module structure reveals a fulcrum for integrin rearrangement upon activation. *Nat Struct Biol* 9: 282–287.
- Xiong JP, Stehle T, Goodman SL, Arnaout MA (2003) New insights into the structural basis of integrin activation. *Blood* 102: 1155–1159.
- Woolf E, Grigorova I, Sagiv A, Grabovsky V, Feigelson SW, et al. (2007) Lymph node chemokines promote sustained T lymphocyte motility without triggering stable integrin adhesiveness in the absence of shear forces. *Nat Immunol* 8: 1076–1085.
- Friedland JC, Lee MH, Boettiger D (2009) Mechanically activated integrin switch controls $\alpha 5\beta 1$ function. *Science* 323: 642–644.
- Kong F, Garcia AJ, Mould AP, Humphries MJ, Zhu C (2009) Demonstration of catch bonds between an integrin and its ligand. *J Cell Biol* 185: 1275–1284.
- Chen W, Lou J, Zhu C (2010) Forcing switch from short- to intermediate- and long-lived states of the αA domain generates LFA-1/ICAM-1 catch bonds. *J Biol Chem* 285: 35967–35978.
- Puklin-Faucher E, Gao M, Schulten K, Vogel V (2006) How the headpiece hinge angle is opened: New insights into the dynamics of integrin activation. *J Cell Biol* 175: 349–360.
- Puklin-Faucher E, Vogel V (2009) Integrin activation dynamics between the RGD-binding site and the headpiece hinge. *J Biol Chem* 284: 36557–36568.
- Gaillard T, Dejaegere A, Stote RH (2009) Dynamics of $\beta 3$ integrin I-like and hybrid domains: insight from simulations on the mechanism of transition between open and closed forms. *Proteins* 76: 977–994.
- Provasi D, Murcia M, Collier BS, Filizola M (2009) Targeted molecular dynamics reveals overall common conformational changes upon hybrid domain swing-out in $\beta 3$ integrins. *Proteins* 77: 477–489.

Author Contributions

Conceived and designed the experiments: WC JL CZ. Performed the experiments: WC JH. Analyzed the data: WC JH. Wrote the paper: WC JL CZ. Provided computational resources: CZ KS SCH.

- Matsumoto A, Kamata T, Takagi J, Iwasaki K, Yura K (2008) Key interactions in integrin ectodomain responsible for global conformational change detected by elastic network normal-mode analysis. *Biophys J* 95: 2895–2908.
- Israelewitz B, Baudry J, Gullingsrud J, Kosztin D, Schulten K (2001) Steered molecular dynamics investigations of protein function. *J Mol Graph Model* 19: 13–25.
- Bell GI (1978) Models for the specific adhesion of cells to cells. *Science* 200: 618–627.
- Lu C, Ferzly M, Takagi J, Springer TA (2001) Epitope mapping of antibodies to the C-terminal region of the integrin $\beta 2$ subunit reveals regions that become exposed upon receptor activation. *J Immunol* 166: 5629–5637.
- Rocco M, Rosano C, Weisel JW, Horita DA, Hantgan RR (2008) Integrin conformational regulation: uncoupling extension/tail separation from changes in the head region by a multiresolution approach. *Structure* 16: 954–964.
- Vomund AN, Stuhlsatz-Krouper S, Dimitry J, Song Y, Frazier WA (2008) A naturally occurring extracellular $\alpha\beta$ clasp contributes to stabilization of $\beta 3$ integrins in a bent, resting conformation. *Biochemistry* 47: 11616–11624.
- Sali A, Blundell TL (1993) Comparative protein modelling by satisfaction of spatial restraints. *J Mol Biol* 234: 779–815.
- Shi M, Foo SY, Tan SM, Mitchell EP, Law SK, et al. (2007) A structural hypothesis for the transition between bent and extended conformations of the leukocyte $\beta 2$ integrins. *J Biol Chem* 282: 30198–30206.
- Case DA, Darden TA, Cheatham TE, III, Simmerling CL, Wang J, et al. (2004) AMBER 8. University of California, San Francisco.
- Jorgensen WL, Chandrasekhar J, Madura JD, Impey RW, Klein ML (1983) Comparison of simple potential functions for simulating liquid water. *J Chem Phys* 79: 926–935.
- Phillips JC, Braun R, Wang W, Gumbart J, Tajkhorshid E, et al. (2005) Scalable molecular dynamics with NAMD. *J Comput Chem* 26: 1781–1802.
- Duan Y, Wu C, Chowdhury S, Lee MC, Xiong G, et al. (2003) A point-charge force field for molecular mechanics simulations of proteins based on condensed-phase quantum mechanical calculations. *J Comput Chem* 24: 1999–2012.
- Kirschner KN, Woods RJ (2001) Quantum mechanical study of the nonbonded forces in water-methanol complexes. *J Phys Chem A* 105: 4150–4155.
- Kirschner KN, Yongye AB, Tschampel SM, Gonzalez-Outeirino J, Daniels CR, et al. (2008) GLYCAM06: a generalizable biomolecular force field. *Carbohydrates*. *J Comput Chem* 29: 622–655.
- Ryckaert JP, Ciccotti G, Berendsen HJC (1977) Numerical-integration of cartesian equations of motion of a system with constraints: molecular dynamics of n-alkanes. *J Comput Phys* 23: 327–341.
- Miyamoto S, Kollman PA (1992) Settle: An analytical version of the SHAKE and RATTLE algorithm for rigid water models. *J Comput Chem* 13: 952–962.
- Darden T, York D, Pedersen L (1993) Particle mesh Ewald: an N-log(N) method for Ewald sums in large systems. *J Chem Phys* 98: 10089–10092.
- Feller SE, Zhang YH, Pastor RW, Brooks BR (1995) Constant pressure molecular dynamics Simulation: The Langevin piston method. *J Chem Phys* 103: 4613–4621.
- Humphrey W, Dalke A, Schulten K (1996) VMD: visual molecular dynamics. *J Mol Graphics* 14: 33–38, 27–38.
- Wriggers W, Schulten K (1997) Protein domain movements: Detection of rigid domains and visualization of hinges in comparisons of atomic coordinates. *Proteins* 29: 1–14.
- Larkin MA, Blackshields G, Brown NP, Chenna R, McGettigan PA, et al. (2007) Clustal W and Clustal X version 2.0. *Bioinformatics* 23: 2947–2948.
- Jain E, Bairoch A, Duvaud S, Phan I, Redaschi N, et al. (2009) Infrastructure for the life sciences: design and implementation of the UniProt website. *BMC Bioinformatics* 10: 136.